Journal of The Electrochemical Society, **150** (3) A249-A256 (2003)
0013-4651/2003/150(3)/A249/8/$7.00 © The Electrochemical Society, Inc.

Measurement of O_2-N_2 Effective Diffusivity in Porous Media at High Temperatures Using an Electrochemical Cell

Feng Zhao,* Tad J. Armstrong, and Anil V. Virkar**,z**

Department of Materials Science and Engineering University of Utah, Salt Lake City, Utah 84112, USA

The effective diffusivity of O_2-N_2 in porous media was measured at high temperatures (650-800°C) using an electrochemical concentration cell. Porous membranes having total porosity between 29 and 48 vol% were fabricated from Sr-doped $LaMnO_3$ (LSM) with 20 to 30 wt% carbon added as a pore former. The O_2-N_2 effective binary diffusivity, $D^{\text{eff}}_{O_2\text{-}N_2}$, at 800°C increased from ~0.016 to ~0.12 cm^2/s with increasing open porosity between 15 and 44 vol%. The $D^{\text{eff}}_{O_2\text{-}N_2}$ exhibited a nonlinear dependence on open porosity and increased dramatically for samples with greater than 35 vol% open porosity. The estimated effective Knudsen diffusivities of O_2 and N_2, $D^{\text{eff}}_{O_2K}$ and $D^{\text{eff}}_{N_2K}$, at 800°C were an order of magnitude higher than the effective binary diffusivity, $D^{\text{eff}}_{O_2\text{-}N_2}$. Thus, O_2-N_2 transport through the porous membranes was governed by the effective binary diffusivity, $D^{\text{eff}}_{O_2\text{-}N_2}$. The effects of O_2-N_2 effective binary diffusivity, $D^{\text{eff}}_{O_2\text{-}N_2}$, on concentration polarization of cathodes for solid oxide fuel cells were assessed. The nonlinear behavior of the O_2-N_2 effective diffusivity as a function of open porosity indicates that a critical amount of porosity in the cathode is necessary to ensure that the overpotential due to concentration polarization is small. The temperature dependence of $D^{\text{eff}}_{O_2\text{-}N_2}$ was investigated between 650 and 800°C, which was found to be in accord with the Chapman-Enskog model.
© 2003 The Electrochemical Society. [DOI: 10.1149/1.1540156] All rights reserved.

Manuscript submitted March 21, 2002; revised manuscript received August 16, 2002. Available electronically January 23, 2003.

The contribution of concentration polarization to the total polarization at both the anode and cathode of solid oxide fuel cells (SOFCs) can be substantial.[1,2] The effects of concentration polarization are most pronounced in electrodes of low porosity and at high current densities. In electrode-supported SOFCs, the contribution of ohmic polarization (IR drop) of a thin electrolyte to the total overpotential of the cell is small as compared to that of an electrolyte-supported SOFC. In fact, anode-supported SOFC have been reported wherein the contribution of the electrolyte ohmic polarization (IR drop) is less than that of the combined polarization losses at the two electrodes. Thus, in the case of electrode-supported SOFCs, the maximum current density attainable is largely limited by polarization losses at the electrodes. In electrode-supported SOFCs, one of the two electrodes, either anode or cathode, is fabricated of a thickness large enough to function as a support and thereby lend mechanical integrity. However, this does not mean that concentration polarization of the support electrode is necessarily greater than that of the thin electrode. For example, anode-supported SOFCs are routinely fabricated with anodes consisting of NiO and YSZ composites that are subsequently reduced *in situ* resulting in highly porous Ni and YSZ cermets. Measurements conducted on anode-supported SOFCs show that overpotential at the thick anode can often be less than that at the thin cathode. Typically, cathodes are fabricated from an electrocatalyst such as Sr-doped $LaMnO_3$ or Sr-doped $LaCoO_3$. In order to generate some porosity, a pore former is typically added and the cathode is fired at temperatures high enough to partially sinter the electrocatalyst, without in the process reducing porosity. However, the amount of porosity necessary to ensure that the concentration polarization is sufficiently small in a cathode at operating temperatures is not very well understood.

Concentration polarization at the cathode is related to the resistance to transport of oxygen gas to the physically distinct cathode/electrolyte interface. Concentration polarization at a given current density depends upon the partial pressure of oxygen in the oxidant, cathode porosity, pore size, and thickness. The cathode-limited current density arises when the partial pressure of oxygen at the cathode/electrolyte interface is nearly zero. For values of current density lower than the limiting current density, the partial pressure of oxygen at the cathode/electrolyte interface is finite (greater than zero). Under such conditions, the current density is proportional to the difference in partial pressures of oxygen in the cathode chamber (outside the cathode), and that at the cathode/electrolyte interface; with the proportionality constant which includes the effective binary diffusivity of O_2-N_2, $D^{\text{eff}}_{O_2\text{-}N_2}$.

Substantial concentration polarization may well arise from the cathode. Thus, it is desirable to measure the effective O_2-N_2 diffusivity in porous media at high temperatures. A considerable amount of work in the field of experimental and theoretical treatments of the effective diffusivity in porous media has been reported in the open literature.[3,4] Gas transport in porous media is complex and includes contributions from bulk, Knudsen,[a] and surface diffusion, as well as viscous flow. The analysis of gas flow is further complicated by interactions with pore structure, for example adsorption/desorption processes on the internal surfaces of porous media. The effective diffusivity of mixed gases has been measured using techniques including gas chromatography (GC),[5,6] steady-state diffusion cells, transient diffusion cells, thermogravimetry using a microbalance,[7] and zero-length columns.[8] Measurements of effective diffusivity by all of these methods are conducted at a pressure of one atmosphere and in the temperature range from 30 to 300°C. From the standpoint of SOFCs, however, the more interesting value of O_2-N_2 effective diffusivity is that measured at 800°C, which is the typical operating temperature of anode-supported SOFCs.

In this study, the effective binary diffusivity of O_2-N_2 through porous media was measured over a range of temperatures between 650 and 800°C using an electrochemical concentration cell. Measurements were conducted on porous discs of Sr-doped $LaMnO_3$ with total porosity ranging between 29 and 48%. The electrochemical cell allowed for an accurate control of the oxygen partial pressure within the sealed cell chamber. Thus, one side of the porous membrane was exposed to ambient conditions (p_{O_2} = 0.21 atm) while the oxygen partial pressure on the other side was carefully regulated with the concentration cell. The effective binary diffusivity of O_2-N_2 was calculated based on the measured oxygen flux through the porous membrane under steady-state conditions.

* Electrochemical Society Student Member.
** Electrochemical Society Active Member.
z E-mail: anil.virkar@m.cc.utah.edu

[a] In Knudsen diffusion dominated flow, the pore radius (assumed cylindrical) is equal to or less than the molecular mean free path, such that gas molecules collide more frequently with pore walls than with other molecules.

Downloaded on 2016-09-17 to IP 130.203.136.75 address. Redistribution subject to ECS terms of use (see ecsdl.org/site/terms_use) unless CC License in place (see abstract).

Theoretical Analysis

Analysis of gas transport through porous bodies can be done using the method of effective diffusivities, which explicitly accounts for pore volume and tortuosity, or using the Dusty gas model, in which the material comprising the solid part of the porous body is treated as an additional gaseous species with enormous mass, and thus is effectively immobile.[9] In what follows, we will use the method of effective diffusivities.

Isothermal, binary transport of O_2 and N_2 through a porous medium can be phenomenologically described by the following equations (wherein 1 denotes O_2 and 2 denotes N_2)[9]

$$J_1 = -D_1\nabla n_1 + X_1\delta_1 J - X_1\gamma_1\left(\frac{nB_o}{\mu}\right)\nabla p \quad [1]$$

$$J_2 = -D_2\nabla n_2 + X_2\delta_2 J - X_2\gamma_2\left(\frac{nB_o}{\mu}\right)\nabla p \quad [2]$$

where

$$\delta_1 = \frac{D_{1K}^{eff}}{D_{1K}^{eff} + D_{12}^{eff}} \quad \text{and} \quad \delta_2 = \frac{D_{2K}^{eff}}{D_{2K}^{eff} + D_{12}^{eff}} \quad [3]$$

$$\gamma_1 = 1 - \delta_1 = \frac{D_{12}^{eff}}{D_{1K}^{eff} + D_{12}^{eff}} \quad \text{and} \quad \gamma_2 = 1 - \delta_2 = \frac{D_{12}^{eff}}{D_{2K}^{eff} + D_{12}^{eff}} \quad [4]$$

$$\frac{1}{D_1} = \frac{1}{D_{1K}^{eff}} + \frac{1}{D_{12}^{eff}} \quad \text{and} \quad \frac{1}{D_2} = \frac{1}{D_{2K}^{eff}} + \frac{1}{D_{12}^{eff}} \quad [5]$$

where n_1 and n_2 are the concentrations of 1 and 2 (in no. per cubic meter or no. per cubic centimeter), respectively, X_1 and X_2 are the mole fractions of 1 and 2, respectively, n is the total concentration, μ is viscosity (Pa s or dyne s), B_o is permeability (m^2 or cm^2), P is total pressure (N/m^2 or dyne/cm^2), J_1 and J_2 are the fluxes of 1 and 2, respectively, J is the total flux, D_{1K}^{eff} and D_{2K}^{eff} are the effective Knudsen diffusivities of 1 and 2, respectively (m^2/s or cm^2/s), and D_{12}^{eff} is the effective binary diffusivity. The effective Knudsen diffusivities, D_{1K}^{eff} and D_{2K}^{eff}, are related to the Knudsen diffusivities D_{1K} and D_{2K} by

$$D_{1K}^{eff} = \frac{D_{1K}V_v}{\tau} \quad \text{and} \quad D_{2K}^{eff} = \frac{D_{2K}V_v}{\tau} \quad [6]$$

where V_v is the volume percent of porosity and τ is the tortuosity factor.

If the pore size is sufficiently large, the effects of Knudsen diffusion may be neglected. Thus, if D_{1K}^{eff} and $D_{2K}^{eff} \gg D_{12}^{eff}$, the flux equations reduce to

$$J_1 = -D_{12}^{eff}\nabla n_1 + X_1 J - \frac{X_1 n D_{12}^{eff}}{D_{1K}^{eff}}\frac{B_0}{\mu}\nabla p \quad [7]$$

$$J_2 = -D_{12}^{eff}\nabla n_2 + X_2 J - \frac{X_2 n D_{12}^{eff}}{D_{2K}^{eff}}\frac{B_0}{\mu}\nabla p \quad [8]$$

In the above, we have replaced $D_{1K}^{eff} + D_{12}^{eff}$ and $D_{2K}^{eff} + D_{12}^{eff}$ by, respectively, D_{1K}^{eff} and D_{2K}^{eff}. Consider the application of above equations to an SOFC cathode. When an SOFC is operated under load, a net current density flows through the cell. The corresponding flux of molecular oxygen flows from the cathodic chamber, through the porous cathode, to the cathode/electrolyte interface, where oxygen molecules are converted into oxygen ions, and are incorporated into the electrolyte for further transport towards the anode. In a steady state, the partial pressure of oxygen at the cathode/electrolyte interface will be fixed, and will be a function of porosity, tortuosity factor, thickness, and the current density. The transport of oxygen through the porous cathode can then be described by Eq. 7. The flux of nitrogen, similarly, is described by Eq. 8. However, no net transport of nitrogen can occur through the electrolyte, as the electrolyte only conducts oxygen ions. Under a steady state, therefore, nitrogen flux must be zero everywhere. That is, under a steady state, $J_2 = 0$ since the nitrogen flux is zero. Thus, Eq. 7 can be rewritten as

$$J_1 = -D_{12}^{eff}\nabla n_1 + X_1 J_1 - \frac{X_1 n D_{12}^{eff}}{D_{1K}^{eff}}\frac{B_o}{\mu}\nabla p \quad [9]$$

and Eq. 8 as

$$0 = -D_{12}^{eff}\nabla n_2 + X_2 J_1 - \frac{X_2 n D_{12}^{eff}}{D_{2K}^{eff}}\frac{B_o}{\mu} \quad [10]$$

Adding Eq. 9 and 10,

$$J_1 = -D_{12}^{eff}\nabla(n_1 + n_2) + (X_1 + X_2)J_1 - \frac{X_1 n D_{12}^{eff}}{D_{1K}^{eff}}\frac{B_o}{\mu}\nabla p - \frac{X_2 n D_{12}^{eff}}{D_{2K}^{eff}}\frac{B_o}{\mu}\nabla p \quad [11]$$

Assuming the applicability of the ideal gas equation of state, we have

$$n_1 = \frac{p_1}{k_B T}, \quad n_2 = \frac{p_2}{k_B T} \quad \text{and} \quad n = n_1 + n_2 = \frac{p_1}{k_B T} + \frac{p_2}{k_B T} = \frac{p}{k_B T} \quad [12]$$

where, k_B is the Boltzmann constant. We also know that $X_1 + X_2 = 1$. Substitution into Eq. 11 gives

$$0 = \left[\frac{D_{12}^{eff}}{k_B T} + \frac{X_2 n D_{12}^{eff}}{D_{2K}^{eff}}\frac{B_0}{\mu} + \frac{X_1 n D_{12}^{eff}}{D_{1K}^{eff}}\frac{B_0}{\mu}\right]\nabla p \quad [13]$$

Equation 13 implies that $\nabla p = 0$ and the flux equations reduce to

$$J_1 = -D_{12}^{eff}\nabla n_1 + X_1 J_1 \quad [14]$$

or

$$J_1 = \frac{-D_{12}^{eff}}{(1 - X_1)}\nabla n_1 \quad [15]$$

Using Eq. 12, the flux J_1 is given by

$$J_1 = \frac{-D_{12}^{eff}}{k_B T}\frac{p}{(p - p_1)}\nabla p_1 \quad [16]$$

The flux of oxygen molecules, J_1 (mol cm^{-2} s^{-1}) is related to current density by

$$J_1 = \frac{i}{4F} \quad [17]$$

where i is current density and F is the Faraday constant. Substitution into Eq. 16 for one-dimensional transport gives

$$\frac{iN_A k_B T dx}{4FD_{12}^{eff} p} = \frac{-dp_1}{(p - p_1)} \quad [18]$$

Downloaded on 2016-09-17 to IP 130.203.136.75 address. Redistribution subject to ECS terms of use (see ecsdl.org/site/terms_use) unless CC License in place (see abstract).

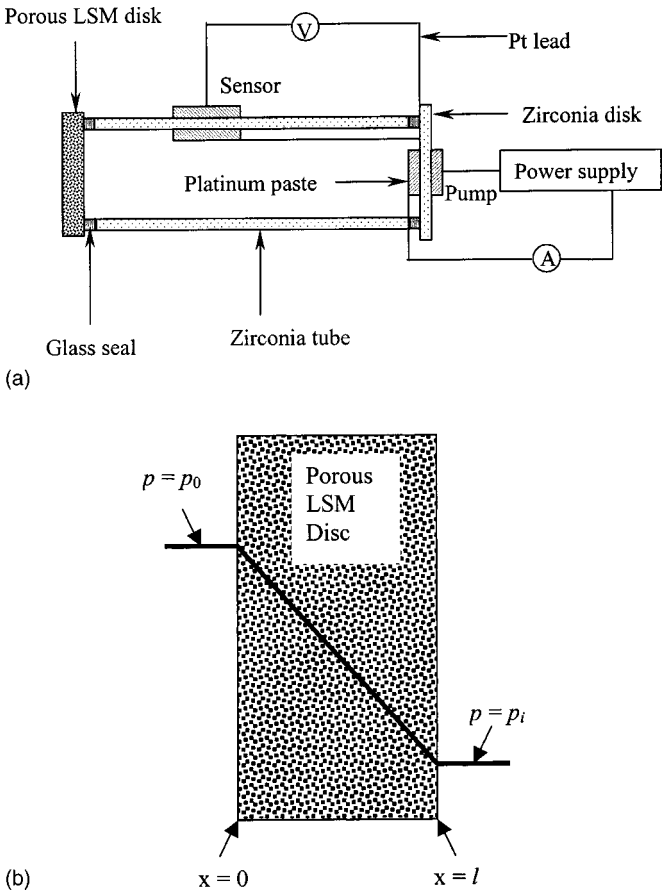

Figure 1. (a) A schematic of the electrochemical cell used to measure the effective binary diffusivity, $D^{\text{eff}}_{O_2\text{-}N_2}$, in porous samples. (b) A schematic of a LSM porous disc, along with partial pressures of oxygen.

where N_A is Avogadro's number. In an actual SOFC, it is not possible to measure the partial pressure of oxygen at the cathode/electrolyte interface. However, transport characteristics of the cathode can be independently and experimentally investigated by an electrochemical cell of the type shown in Fig. 1a, which is a schematic of the electrochemical cell used in this study for the measurement of the O_2-N_2 effective diffusivity. The electrochemical cell consists of a disc of an oxygen-ion-conducting material (*e.g.*, yttria-stabilized zirconia, YSZ), sealed to a YSZ cylinder using a suitable glass. Platinum electrodes are applied to both the disc as well as part of the cylinder, as shown in Fig. 1a. At the other end, a porous disc of a prospective cathode is attached, again using a suitable glass. The entire assembly is heated to an elevated temperature, and a direct current voltage is applied across the electrodes on the YSZ disc, so as to pump out oxygen from the cylinder. As the partial pressure of oxygen in the cylinder (p_i or pO_2) is lowered, oxygen from the ambient diffuses through the porous disc, into the chamber (cylinder). Under a steady state, the pO_2 in the cylinder is lower than that in the ambient. This pO_2 can be measured electrochemically using the electrodes applied to the YSZ cylinder, which serve as sensing electrodes. The flux of oxygen through the porous disc is described by the preceding equations. Also, as no nitrogen can transport through the YSZ disc, it is clear that under a steady state, no transport of nitrogen occurs through the porous disc. In this sense, the electrochemical cell simulates conditions experienced by an SOFC cathode, with the opportunity to precisely know what the pO_2 in the cylinder is; or what the pO_2 at the cathode/electrolyte interface is in an actual SOFC, under a given set of conditions.

Figure 1b shows a schematic of a porous LSM disc, with the thickness and the partial pressures of oxygen labeled. From Fig. 1b, when $x = 0$, the oxygen partial pressure outside of the zirconia tube is, $p_1 = p_0$, and when $x = l$, the oxygen partial pressure inside of the zirconia tube is $p_1 = p_i$, and p = total pressure. Integration of Eq. 18 gives

$$p_i = p - (p - p_0)\exp\left[\frac{iRTl}{4FD^{\text{eff}}_{12}p}\right] \qquad [19]$$

where R is the ideal gas constant. Since the thickness of the porous Sr-doped $LaMnO_3$ (LSM) disk is small, the exponent can be shown to be much less than one, for most current densities of interest. Then Eq. 19 can be simplified as

$$p_i \approx p_0 - \left(\frac{p - p_0}{p}\right)\left[\frac{iRTl}{4FD^{\text{eff}}_{12}}\right] \qquad [20]$$

Substituting for $i/4F$ with J in Eq. 20 gives

$$J \approx -\left[\left(\frac{p}{p - p_0}\right)\left(\frac{D^{\text{eff}}_{12}}{RTl}\right)\right](p_i - p_0) = \left(\frac{pp_0}{p - p_0}\right)\left(\frac{D^{\text{eff}}_{12}}{RTl}\right) - \left(\frac{p}{p - p_0}\right)\left(\frac{D^{\text{eff}}_{12}}{RTl}\right)p_i \qquad [21]$$

where $p = 1$ atm (1.013×10^5 N/m^2), $p_0 = 0.21$ atm (2.128×10^4 N/m^2), p_i is the oxygen partial pressure inside the electrochemical cell, l is the thickness of the porous LSM disk, T is the operating temperature, and D^{eff}_{12} is the O_2-N_2 effective binary diffusivity, $D^{\text{eff}}_{O_2\text{-}N_2}$.

From the slope of oxygen flux through the porous LSM sample as a function of partial pressure of oxygen inside the cell, p_i, the O_2-N_2 effective diffusivity, $D^{\text{eff}}_{O_2\text{-}N_2}$, through the porous disc can be calculated. Equation 21 shows that the $D^{\text{eff}}_{O_2\text{-}N_2}$ can also be obtained from the intercept.

Experimental Procedure

Fabrication of porous LSM discs.—Porous samples in the shape of discs were fabricated from $La_{0.85}Sr_{0.15}MnO_3$ powder (Praxair), mixed with 20, 22.5, 25, 27.5, and 30% (by weight) carbon (HTW). Carbon particles were spherical with a particle size ranging between 20 and 50 μm in diam. The powder mixtures were wet-milled, dried, and then screened. Discs of diam ~20 mm and thickness ~1 mm

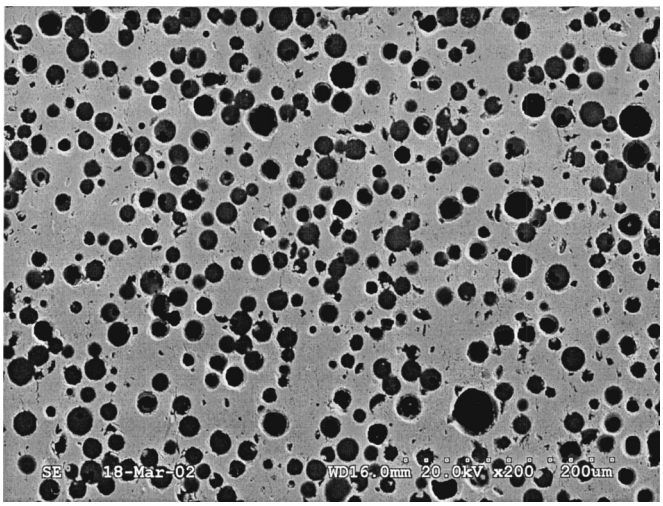

Figure 2. A scanning electron micrograph (SEM) of a porous LSM disc fabricated with 27.5 wt% carbon.

Downloaded on 2016-09-17 to IP 130.203.136.75 address. Redistribution subject to ECS terms of use (see ecsdl.org/site/terms_use) unless CC License in place (see abstract).

Table I. Density and volume percent of porosity of LSM samples fabricated with various weight percents of carbon.

(wt%) Carbon	Density (g/cm^3)	Total porosity by SEM (vol%)	Total porosity (vol%)	Open porosity (vol%)	Closed porosity (vol%)	Fraction of open to total porosity
20	4.64	26.3	28.89	15.42	13.40	0.53
22.5	4.33	32.2	33.69	24.45	9.20	0.72
25	3.98	38.5	39.00	34.66	4.30	0.88
27.5	3.63	42.2	44.44	40.30	4.10	0.91
30	3.41	45.3	47.70	43.77	3.90	0.92

were uniaxially die-pressed and then fired at 1200°C for 1 h in air. The microstructure and porosity of the samples were evaluated using scanning electron microscopy (SEM). The open, closed, and total porosity of the samples was measured by the Archimedes technique in accordance with ASTM standard C 20-00.

Design and construction of the diffusivity measurement setup.—The O_2-N_2 effective diffusivity through the porous discs was measured using an electrochemical concentration cell. The cell was fabricated using a dense, 8 mol% YSZ cylindrical tube, a dense YSZ disc, and a porous LSM disc, as shown in Fig. 1a. Platinum electrodes, in the form of a paste, were applied on both sides of the YSZ disc, and both sides of the YSZ cylinder, on part of the surface. Platinum wire leads were attached to both sets of platinum electrodes. The YSZ cylinder and disc were heated to 750°C for 1 h to ensure that the platinum wire and paste were well adhered to the YSZ disc and the YSZ cylinder. A glass frit (Specialty Glass, Inc.) was mixed with an organic binder to form a paste. The paste was applied between the YSZ cylinder (edge) and disc and the assembly was fired at 850°C for 4 h to form a leak-tight seal. The porous LSM disk was sealed to the other end of the YSZ cylinder using the same procedure. This completed the fabrication of the electrochemical cell.

Electrochemical measurements.—The electrochemical cell was placed in a furnace and measurements were conducted over a range of temperatures between 650 and 800°C. The platinum leads from the YSZ disc were attached to a constant voltage/current dc power supply. In this manner, oxygen could be electrochemically pumped in or out of the cell, depending upon the polarity. The applied current from the power source was monitored using a Keithly model 2000 multimeter. The oxygen pump was operated in both directions to either pump oxygen in or out of the cell. The platinum leads from the zirconia cylinder were connected to a Keithly model 2000 multimeter linked to a computer with LabView software for data acquisition. The Nernst potential of the oxygen sensor was continuously measured. Thus, the partial pressure of oxygen inside the cell was known as a function of time. In terms of the measured Nernst potential, E, and the oxygen partial pressure in the ambient, p_0, the oxygen partial pressure in the chamber, p_i, is given by

$$p_i = p_0 \exp\left[-\frac{4FE}{RT}\right] \qquad [22]$$

When the applied polarity is such that oxygen is electrochemically pumped out, the E is positive and $p_i < p_0$. During testing, a constant current was applied to the pump and the Nernst voltage was monitored until the oxygen partial pressure inside the cell reached a stable (steady state) value. Testing was repeated with the oxygen sensor placed in various locations to ensure that the oxygen partial pressure gradient in the zirconia tube was negligible. The oxygen partial pressure inside the cell was controlled by varying the magnitude of the current applied to the oxygen pump.

Results and Discussion

Microstructural characterization of porous discs.—Figure 2 shows an SEM micrograph of a porous LSM sample in which 27.5 wt% carbon was added to the powder prior to sintering. The size of the pores, as estimated from the micrographs, varied between 1.5 and 50 μm in diam, with the mean pore size (diameter) being approximately 10 to 15 μm in diam. The smaller pores are the result of the breakage of large carbon particles during the milling process. Very small pores are the result of partial sintering, and the corresponding pore sizes are related to the LSM particle size.

The density, and open, closed, and total porosities of the LSM discs fabricated with 20 to 30 wt% carbon, as measured by the Archimedes technique, are presented in Table I. In addition, the total porosity, as calculated by SEM image analysis (systematic point count), is also listed in Table I. With increasing amounts of carbon from 20 to 30 wt%, the density decreases from 4.64 to 3.41 g/cm^3, the total porosity increases from 28.9 to 47.7%, and the open porosity increases from 15.4 to 43.7%. The amount of closed porosity decreases from 13.4 to 4.3% with increasing carbon content from 20 to 25 wt%, and then remains relatively constant at higher carbon concentrations. Thus, there appears to be a critical amount of carbon necessary to ensure that most of the porosity is open.[b] For the given morphology of carbon and resulting pore shape and size, this critical amount lies between 22.5 and 25.0 wt%. At carbon contents greater than or equal to 25 wt%, approximately 90% of the total porosity is open.

The effect of porosity on the effective binary diffusivity of O_2-N_2.—The effective binary diffusivity, $D^{\text{eff}}_{O_2\text{-}N_2}$, was determined by measuring the oxygen flux through porous samples as a function of oxygen partial pressure gradient across the sample. For each flux measurement, a constant current was applied, and maintained until the electrochemical cell reached a steady state, before proceeding to the next measurement. Figure 3 shows a typical plot of Nernst potential as a function of time for a porous disc sample with 24.4% open porosity. The pump current was set at 106.6 mA and the cell reached steady state in approximately 5 min. The plots of oxygen flux as a function of oxygen partial pressure in the cell (inside the YSZ cylinder) for porous LSM samples fabricated with 20 to 30 wt% carbon are shown in Fig. 4. The oxygen flux as a function of oxygen partial pressure, p_i, in the cell, exhibits linear behavior over the range of p_i measured. Linear dependence of oxygen flux on p_i suggests that the simplification given in Eq. 21 is valid, and that over the range of measurements, $D^{\text{eff}}_{O_2\text{-}N_2}$, for a given sample is essentially a constant. The O_2-N_2 binary effective diffusivity, $D^{\text{eff}}_{O_2\text{-}N_2}$, for transport through the porous samples was determined using Eq. 21, both from the slope as well as the intercept. The corresponding results are listed in Table II. Note that with the exception of the sample with the lowest porosity, the $D^{\text{eff}}_{O_2\text{-}N_2}$ measured from both the slope and the intercept, are virtually identical. This demonstrates the validity of the analysis, and the experimental procedure. At the lowest porosity, the value estimated from the intercept is somewhat greater. In the following discussion, the values of

[b] It is to be emphasized that this conclusion concerning the required amount of carbon is valid only for sintered LSM discs, as in the current study, and not for cathode, as applied on SOFC. This is because in the case of discs, sintering is not constrained. However, in a typical SOFC, the cathode is applied over an already fabricated cell, which leads to constrained sintering, and thus greater porosity.

Downloaded on 2016-09-17 to IP 130.203.136.75 address. Redistribution subject to ECS terms of use (see ecsdl.org/site/terms_use) unless CC License in place (see abstract).

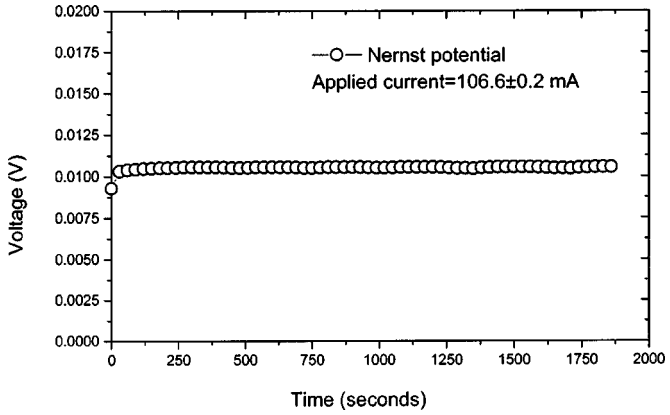

Figure 3. The measured Nernst potential across the oxygen sensor as a function of time, under a constant applied current to the pump made using a LSM disc with 24.4% porosity. Measurement conducted at 800°C.

$D^{\text{eff}}_{O_2\text{-}N_2}$ estimated from the slope are used. The effective diffusivity increases from 0.016 to 0.12 cm^2/s with increasing porosity in the range 15.4 to 43.8%. The dependence of O_2-N_2 effective binary diffusivity on open porosity is nonlinear, as shown in Fig. 5.

The total gas transport through a porous sample should contain contributions from bulk diffusion, Knudsen diffusion, and viscous flow (Eq. 1 and 2), in addition to surface diffusion and adsorption/desorption-related effects. In the preceding, it was assumed that the effective Knudsen diffusivities ($D^{\text{eff}}_{O_2K}$, $D^{\text{eff}}_{N_2K}$) are much larger than the effective binary diffusivity ($D^{\text{eff}}_{O_2\text{-}N_2}$). With this assumption, the pressure gradient across the sample was shown to be equal to zero ($\nabla p = 0$) resulting in no viscous flow through the porous cathode. Thus, the effective diffusivity, $D^{\text{eff}}_{O_2\text{-}N_2}$, calculated from Eq. 21 is valid if the Knudsen diffusion in the porous LSM samples can be neglected, and effects due to surface diffusion and adsorption/desorption processes are small.

The important parameters in determining the relative contributions of Knudsen and bulk diffusion to total diffusion are the pore size and the mean free path of the gaseous species. Bulk diffusivity is a function of the molecular velocity (υ) and the mean free path λ as given by[10]

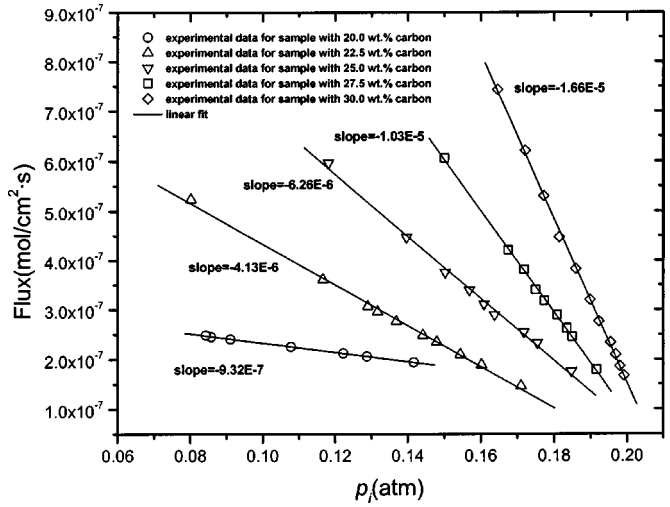

Figure 4. Oxygen flux through porous LSM discs fabricated with varying amounts of carbon, between 20.0 and 30.0 wt%, as a function of oxygen partial pressure inside the cell. Measurement conducted at 800°C.

Table II. Measured effective diffusivity, open porosity, tortuosity, and effective O_2 and N_2 Knudsen diffusivity for LSM samples fabricated with various amounts of carbon.

Carbon (wt%)	$D^{\text{eff}}_{O_2\text{-}N_2}$ From the slope (cm^2/s)	$D^{\text{eff}}_{O_2\text{-}N_2}$ From the intercept (cm^2/s)	Open porosity	Tortuosity	$D^{\text{eff}}_{O_2K}$ (cm^2/s)	$D^{\text{eff}}_{N_2K}$ (cm^2/s)
20	0.016	0.027	15.42	19.7	0.22	0.235
22.5	0.028	0.027	24.43	18.3	0.375	0.401
25	0.046	0.046	34.66	15.6	0.624	0.667
27.5	0.071	0.07	40.30	11.8	0.959	1.025
30	0.117	0.117	43.77	7.8	1.576	1.684

$$D_{12} = \frac{1}{3}\upsilon\lambda \qquad [23]$$

Knudsen diffusivity is dependent on the molecular velocity (υ) and the radius a of a cylindrical pore as given by[10]

$$D_K = \frac{2}{3}\upsilon a \qquad [24]$$

The mean free path λ of many gases at one atmosphere is usually on the order of 100 nm at the temperature of interest (~800°C).[11] For the porous LSM samples (Fig. 2) the mean pore radius, as measured from micrographs, is about 5 μm.[c] Thus, as given by Eq. 23 and 24, $D^{\text{eff}}_{O_2K}$ and $D^{\text{eff}}_{N_2K}$ will be an order of magnitude greater than $D^{\text{eff}}_{O_2\text{-}N_2}$. Therefore, at a total pressure of 1 atmosphere, bulk diffusion should dominate and the assumption that Knudsen diffusion can be neglected appears to be valid.

In the phenomenological theory of diffusion through porous bodies, the O_2-N_2 effective diffusivity, $D^{\text{eff}}_{O_2\text{-}N_2}$, is related to the O_2-N_2 binary bulk diffusivity by[12]

$$D^{\text{eff}}_{O_2\text{-}N_2} = \frac{V_V}{\tau} D_{O_2\text{-}N_2} \qquad [25]$$

where V_V is the volume percent of porosity and τ is the tortuosity factor. The experimentally measured tortuosity factor is an all-encompassing term that includes the effects of pore microstructure such as pore orientation, morphology, contiguity, and size, as well as possible adsorption/desorption processes, and surface diffusion, etc., on gas transport. The volume percent of porosity accounts for the fact that gas transport occurs only through the pores and not through the solid matrix.

The bulk diffusivity of a binary gas system at moderate temperatures and pressures can be accurately determined by the Chapman-Enskog relation[12] given as

$$D_{O_2\text{-}N_2} = \frac{0.00186T^{\frac{3}{2}}\left(\frac{1}{M_{O_2}} + \frac{1}{M_{N_2}}\right)^{\frac{1}{2}}}{p\sigma^2_{O_2\text{-}N_2}\Omega} \qquad [26]$$

in cm^2/s where M_{O_2} and M_{N_2} are the molecular weights of the two gaseous species, Ω is the collision integral, $\sigma_{O_2\text{-}N_2}$ is the average collision diameter, and p is the total pressure. The collision diameter $\sigma_{O_2\text{-}N_2}$, given in angstroms, is the arithmetic average of the diameters of the two species present

[c] The bottlenecks are almost certainly smaller than pore radii determined from micrographs. Thus, the above leads to an overestimate of the Knudsen diffusivity.

Downloaded on 2016-09-17 to IP 130.203.136.75 address. Redistribution subject to ECS terms of use (see ecsdl.org/site/terms_use) unless CC License in place (see abstract).

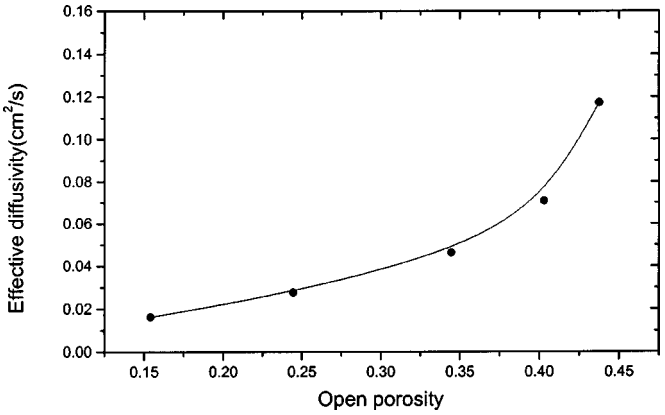

Figure 5. Effective binary diffusivity, $D^{eff}_{O_2\text{-}N_2}$, *vs.* open porosity.

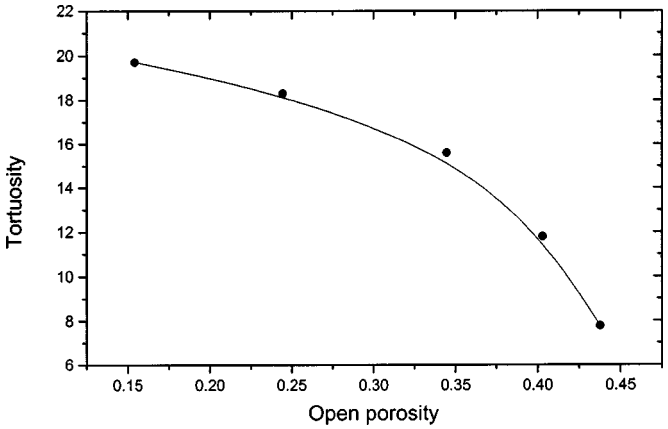

Figure 6. Tortuosity factor *vs.* open porosity.

$$\sigma_{O_2\text{-}N_2} = \frac{1}{2}(\sigma_{O_2} + \sigma_{N_2}) \quad [27]$$

The collision integral Ω is a dimensionless quantity that accounts for interaction between the two gaseous species via the Lennard-Jones potential. For the binary gas system of O_2-N_2 at 800°C, the collision integral is close to unity.[12] The bulk diffusivity of O_2-N_2 as determined by Eq. 26, is approximately 2.08 cm^2/s at 800°C and 1 atm.

Based on the calculated O_2-N_2 bulk diffusivity (Eq. 26), the measured effective O_2-N_2 diffusivity (Table II), and the volume percent of porosity (Table I), the tortuosity factor, τ, can be estimated by Eq. 25. The calculated tortuosity factors for the porous LSM samples fabricated with 20 to 30 wt% carbon are presented in Table II. The tortuosity factor decreases from a value of 19.7 to 7.8 with increasing carbon content from 20 to 30 wt%. The tortuosity factor decreases with increasing open porosity in a nonlinear manner as shown in Fig. 6. Typically, the tortuosity factor of porous media lies between 2 and 6, but values as high as 10 have been reported.[11] The estimated tortuosity factors of the LSM samples fabricated with 20, 22.5, and 25 wt% carbon were high with values ranging between 15.6 and 19.7. Such high values of tortuosity factors are probably the result of neglecting Knudsen diffusion, surface diffusion and adsorption/desorption processes. It is quite possible that the dimensions of bottlenecks in the pore structure may be considerably smaller than the estimated average size of pores from SEM micrographs. This would mean that the actual Knudsen diffusivities are probably smaller than assumed, and high tortuosity factors are the result of neglecting the effects of Knudsen diffusion.

For evaluating the Knudsen diffusivity given in Eq. 24, the following expression was used to determine the mean molecular velocity of a gas species in a mixture[11]

$$\upsilon_1 = \sqrt{\frac{8RT}{\pi M_1}} \quad [28]$$

where M_1 is the molecular weight of component 1 in a mixture.

Combining Eq. 24 with Eq. 28 gives

$$D_K = \frac{2}{3} a \sqrt{\frac{8RT}{\pi M_1}} \quad [29]$$

Combining Eq. 25 with Eq. 29 gives the effective Knudsen diffusivity for each gaseous species in the mixture

$$D^{eff}_{1K} = \frac{2}{3} a \sqrt{\frac{8RT}{\pi M_1}} \frac{V_v}{\tau} \quad [30]$$

and

$$D^{eff}_{2K} = \frac{2}{3} a \sqrt{\frac{8RT}{\pi M_2}} \frac{V_v}{\tau} \quad [31]$$

where M_1 and M_2 are the molecular weights of gaseous species 1 and 2, respectively.

Knowing the tortuosity factor, the effective Knudsen diffusivities of both O_2 and N_2 through the porous LSM samples can be determined by Eq. 30 and 31 assuming some pore radius. In the present work, the pore size was estimated from SEM micrographs. However, the actual pore bottlenecks are almost certainly smaller. Thus, the present calculations of Knudsen diffusivities are overestimates.

The calculated O_2 and N_2 effective Knudsen diffusivities for the porous LSM samples at 800°C and 1 atm are listed in Table II. The calculated Knudsen diffusivities increase from 0.23 to 1.68 for the samples fabricated from 20 to 30 wt% carbon. For all samples, both the $D^{eff}_{O_2K}$ and $D^{eff}_{N_2K}$ are an order of magnitude greater than $D^{eff}_{O_2\text{-}N_2}$, which is consistent with the original assumption. However, it is to be emphasized that the actual bottlenecks may be smaller than the assumed pore sizes. If this is the case, large tortuosity factors estimated for samples of lower porosity may principally be the result of neglecting the effects of Knudsen diffusion.

The temperature dependence of the effective binary diffusivity of O_2-N_2.—The effective diffusivities of O_2-N_2 through porous media at various temperatures were measured. The effective diffusivities for the samples fabricated with 22.5 carbon and 27.5 wt% carbon at temperatures between 650 and 800°C are listed in Table III. As seen in the table, the $D^{eff}_{O_2\text{-}N_2}$ increases with increasing temperature. The increase in effective diffusivity with temperature is due to the increase in the average molecular velocity and the mean free path. As a function of temperature, T, the average molecular velocity follows a $T^{0.5}$ dependence and the mean free path is linear with T. Thus, the effective diffusivity should exhibit a $T^{1.5}$ dependence. The effective diffusivity for both samples plotted as a function of $T^{1.5}$ is shown in Fig. 7. The effective diffusivities are linear with respect to

Table III. Measured effective diffusivity as a function of temperature for two LSM disks with different amounts of porosity.

	$D^{eff}_{O_2\text{-}N_2}$ (cm^2/s)	
Temperature (°C)	Sample fabricated with 22.5 wt% C	Sample fabricated with 27.5 wt% C
650	0.024	0.056
700	0.026	0.062
750	0.029	0.067
800	0.031	0.072

Downloaded on 2016-09-17 to IP 130.203.136.75 address. Redistribution subject to ECS terms of use (see ecsdl.org/site/terms_use) unless CC License in place (see abstract).

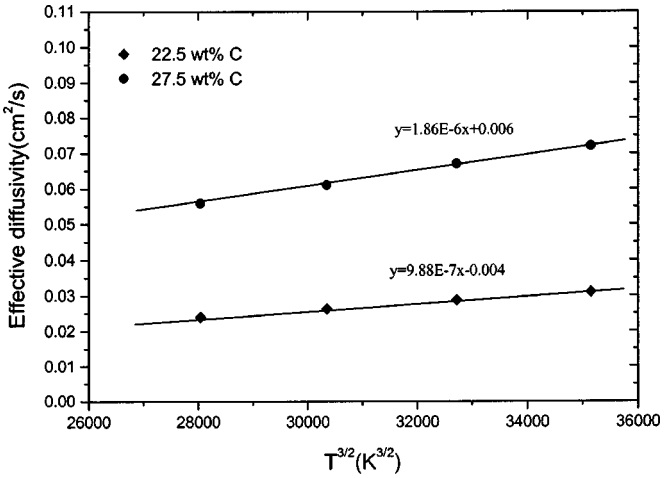

Figure 7. Effective binary diffusivity, $D^{\text{eff}}_{O_2\text{-}N_2}$, as a function of temperature, $T^{1.5}$, for porous LSM disks fabricated with 22.5 and 27.5 wt% carbon.

$T^{1.5}$ consistent with the Chapman-Enskogg relation. The intercept, however, should be zero. The observation that the intercept is non-zero is simply the result of experimental scatter in measurements. The slope of the sample fabricated from 27.5 wt% carbon is greater than that for the sample fabricated from 22.5 wt% carbon by a factor of 2.5. The difference in slopes is partially attributed to the higher percentage of porosity and a lower value of tortuosity in the samples made with 27.5 wt% carbon as compared to the samples made with 22.5 wt% carbon. A comparison of the ratios $\frac{V_V}{\tau}$ for the two samples at 800°C (Table II) shows that they differ by a factor of approximately 1.9.

The limiting current density and concentration polarization.—The limiting current density due to concentration polarization at the cathode is determined by setting Eq. 20 to zero, *i.e.*, $p_i \approx 0$, and is given by

$$i_{cs} \approx \left[\frac{4FD^{\text{eff}}_{O_2\text{-}N_2}}{RTl}\right] p_o \left(\frac{p}{p - p_o}\right) \qquad [32]$$

where p_o is the partial pressure of oxygen in the oxidant (air) outside of the cathode (Pa or atm), p is total pressure, $D^{\text{eff}}_{O_2\text{-}N_2}$ is the effective O_2-N_2 diffusion coefficient of the porous cathode (cm^2/s or m^2/s), and l is the cathode thickness (cm or m). If the more accurate equation (Eq. 19) is used instead, the limiting current density is given by

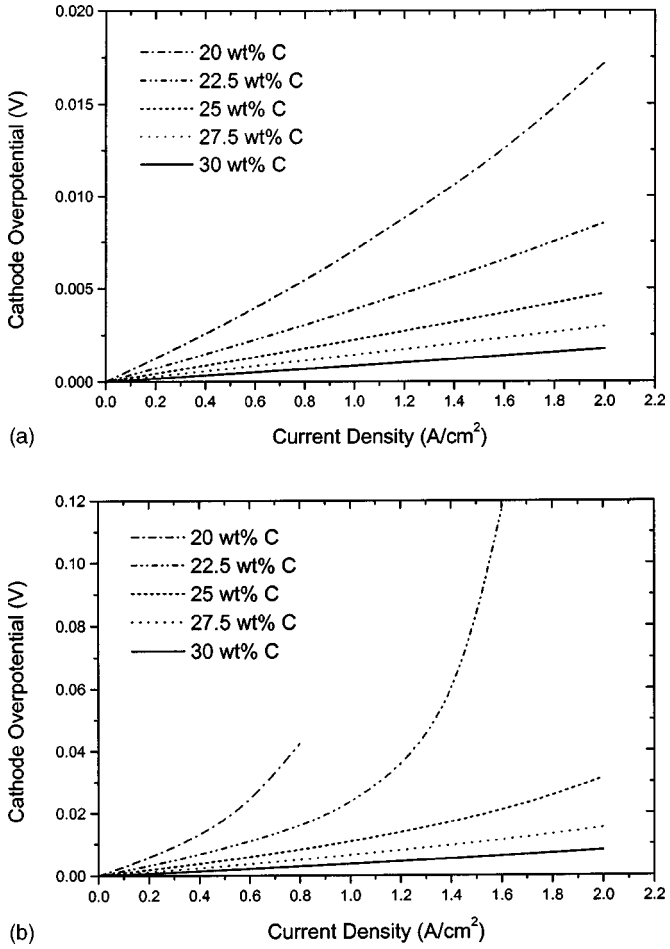

Figure 8. (a) Calculated cathode overpotential as a function of current density for porous LSM cathodes fabricated with 20.0 to 30.0 wt% carbon. Cathode thickness = 50 μm. Cathode-limiting current density calculated using Eq. 32. (b) Calculated cathode overpotential as a function of current density for porous LSM cathodes fabricated with 20.0 to 30.0 wt% carbon. Cathode thickness = 200 μm. Cathode-limiting current density calculated using Eq. 32.

Table IV. Measured effective diffusivity, open porosity, and cathode limiting current density for LSM disks fabricated with various amounts of carbon.

Sample no., percent C	$D^{\text{eff}}_{O_2\text{-}N_2}$ (cm^2/s)	Open porosity (%)	i_{cs} (50 μm)[a] (A/cm^2)	i_{cs} (50 μm)[b] (A/cm^2)	i_{cs} (200 μm)[a] (A/cm^2)	i_{cs} (200 μm)[b] (A/cm^2)
1, 20	0.016	15.42	3.37	3.8	0.84	0.95
2, 22.5	0.028	24.43	5.73	6.46	1.43	1.61
3, 25	0.046	34.66	9.55	10.77	2.38	2.69
4, 27.5	0.071	40.30	14.66	16.53	3.66	4.13
5, 30	0.117	43.77	24.24	27.33	6.05	6.83

[a] Calculated using Eq. 32.
[b] Calculated using Eq. 33.

Downloaded on 2016-09-17 to IP 130.203.136.75 address. Redistribution subject to ECS terms of use (see ecsdl.org/site/terms_use) unless CC License in place (see abstract).

Table V. Calculated cathode overpotential at different cathode thickness for LSM samples fabricated with various amounts of carbon at a current density of 2 A/cm^2.

Thickness (μm)	20 wt% C Cathode overpotential (mV)	22.5 wt% C Cathode overpotential (mV)	25 wt% C Cathode overpotential (mV)	27.5 wt% C Cathode overpotential (mV)	30 wt% C Cathode overpotential (mV)
50	7.1	3.9	2.3	1.4	0.9
100	17.3	8.6	4.8	3.0	1.8
150	36.1	14.5	7.6	4.6	2.7
200	86.2	22.4	10.8	6.4	3.7

$$i_{cs} \approx \left[\frac{4FD^{eff}_{O_2\text{-}N_2}}{RTl}\right] p \ln\left(\frac{p}{p - p_o}\right) \qquad [33]$$

In practice, limiting current densities given by Eq. 32 or 33 often may not be realized since limiting current densities due to either the ohmic contribution or the anodic polarization may smaller. For example, in an electrolyte-supported cell, the ohmic polarization is usually the largest. In such a case, the short circuit current density occurs mainly due to the fact that almost all voltage drop is attributable to the ohmic polarization. The limiting current densities given in Eq. 32 and 33, are useful for estimating the contributions of cathodic concentration polarization as a function current density.

In terms of the limiting current density, i_{cs}, the concentration polarization at the cathode is given as[13]

$$\eta_{conc(c)} = -\frac{RT}{4F} \ln\left(1 - \frac{i}{i_{cs}}\right) \qquad [34]$$

where i is current density (A/cm^2). Assuming that the cathode of an anode-supported SOFC has a similar microstructure as the porous LSM disc samples, the cathode limiting current density and cathode polarization can be estimated by Eq. 32 or 33, and 34. Table IV lists the cathode limiting current densities calculated for different effective diffusivities for cathodes of two different thicknesses; 50 and 200 μm. The cathode concentration overpotential as a function of current density (up to 2 A/cm^2) for cathodes with various effective diffusivities is shown in Fig. 8a and b for cathode thicknesses of 50 and 200 μm, respectively. Note that there is a significant effect of cathode porosity on concentration polarization, especially for the cathode thickness of 200 μm. Thus, the effective diffusivity of O_2-N_2 in porous cathodes can greatly influence the overall performance of a cell.

The effects of cathode thickness and porosity on the cathode overpotential are shown in Table V. The overpotentials were calculated based on the O_2-N_2 effective diffusivities of the porous LSM samples. For the sample fabricated with 20 wt% carbon, the cathode overpotential increases from 7.1 to 86.2 mV with an increase in cathode thickness from 50 to 200 μm for a current density of 2 A/cm^2. On the other hand, for the 30 wt% carbon sample, the cathode overpotential only increases from 0.9 to 3.7 mV when increasing the cathode thickness from 50 to 200 μm. Thus, the adverse effects of increasing cathode thickness on concentration polarization are greatly reduced with adequate porosity.

Conclusions

The present work has developed an electrochemical technique, which affords the measurement of effective binary diffusivities of O_2-N_2, $D^{eff}_{O_2\text{-}N_2}$, through porous media at elevated temperatures. The technique was applied to porous LSM discs containing a range of porosities, and as a function of temperature between 650 and 800°C. The results showed that transport through porous LSM discs could be adequately described by effective binary diffusion. The O_2-N_2 effective binary diffusivity, $D^{eff}_{O_2\text{-}N_2}$, at 800°C increased from ~0.016 to ~0.12 cm^2/s with increasing open porosity between 15 and 44 vol%. Using the values of the effective diffusivities measured, cathodic concentration polarization was estimated. The results show that for relatively thick cathodes (~200 μm), cathodic concentration polarization can be significant, especially at lower porosities. This shows the importance of ensuring that the open porosity in the cathode is adequate. Also using the experimentally measured $D^{eff}_{O_2\text{-}N_2}$, the volume fraction of porosity, and the calculated binary diffusivity by the Chapman-Enskog model, tortuosity factors were estimated. The estimated tortuosity factor ranged between ~7.8 and ~19.7, the latter for samples with relatively low porosity. At high values of porosity, the estimated tortuosity factor (~7.8) may be attributed to the tortuous nature of gas transport. Very high tortuosity factors (such as >10), in samples with a low volume fraction of open porosity, are probably the result of neglecting Knudsen diffusion and surface diffusion. In these samples, it is possible that the pore size, especially the bottlenecks, may be on the order of the mean free path.

Acknowledgments

This work was supported by the U.S. Department of Energy, NETL, contract no. DE- AC26-99FT40713.

The University of Utah assisted in meeting the publication costs of this article.

References

1. K. Z. Fung and A. V. Virkar, in *Solid Oxide Fuel Cells (SOFC-IV)*, M. Dokiya, O. Yamamoto, H. Tagawa, and S. C. Singhal, Editors, PV 95-1, p. 1105, The Electrochemical Society Proceedings Series, Pennington, NJ (1995).
2. T. Kenjo and Y. Yamakoshi, *Bull. Chem. Soc. Jpn.*, **65**, 995 (1992).
3. C. N. Satterfield, *Mass Transfer in Heterogeneous Catalysis*, MIT Press, Cambridge, MA (1970).
4. R. Aris, *The Mathematical Theory of Diffusion and Reaction in Permeable Catalysts*, Clarendon Press, Oxford, U. K. (1975).
5. P. Schneider and J. M. Smith, *AIChE J.*, **14**, 762 (1968).
6. E. Ruckenstein, A. S. Vaidyanathan, and G. R. Youngquist, *Chem. Eng. Sci.*, **25**, 1306 (1971).
7. P. Gray and D. D. Do, *AIChE J.*, **37**, 1027 (1991).
8. J. R. Hufton and D. M. Ruthven, *Ind. Eng. Chem. Res.*, **32**, 2379 (1993).
9. E. A. Mason and A. P. Malinaukus, *Gas Transport in Porous Media: The Dusty Gas Model*, Elsevier, Amsterdam (1983).
10. J. M. Smith, *Chemical Engineering Kinetics*, McGraw-Hill Book Company, New York (1970).
11. F. P. Reif, *Statistical and Thermal Physics*, McGraw-Hill, New York (1975).
12. E. L. Cussler, *Diffusion*: *Mass Transfer in Fluid Systems*, Cambridge University Press, Cambridge, U. K. (1995).
13. J. W. Kim, A. V. Virkar, K.-Z. Fung, K. Metha, and S. C. Singhal, *J. Electrochem. Soc.*, **146**, 69 (1999).

Downloaded on 2016-09-17 to IP 130.203.136.75 address. Redistribution subject to ECS terms of use (see ecsdl.org/site/terms_use) unless CC License in place (see abstract).